Provided for non-commercial research and education use.
Not for reproduction, distribution or commercial use.

Volume 267, Issues 1–2 1 March 2008 ISSN 0012-821X

ELSEVIER

EARTH & PLANETARY SCIENCE LETTERS

This article was published in an Elsevier journal. The attached copy is furnished to the author for non-commercial research and education use, including for instruction at the author's institution, sharing with colleagues and providing to institution administration.

Other uses, including reproduction and distribution, or selling or licensing copies, or posting to personal, institutional or third party websites are prohibited.

In most cases authors are permitted to post their version of the article (e.g. in Word or Tex form) to their personal website or institutional repository. Authors requiring further information regarding Elsevier's archiving and manuscript policies are encouraged to visit:

http://www.elsevier.com/copyright

Author's personal copy

Available online at www.sciencedirect.com
ScienceDirect
Earth and Planetary Science Letters 267 (2008) 69–82
EPSL
www.elsevier.com/locate/epsl

Cooling rates in the lower crust of the Oman ophiolite: Ca in olivine, revisited

Jill A. VanTongeren *, Peter B. Kelemen, Karen Hanghøj

Department of Earth and Environmental Sciences, Columbia University - Lamont-Doherty Earth Observatory, 61 Rt 9W, Palisades, NY 10964, United States

Received 4 July 2007; received in revised form 5 October 2007; accepted 17 November 2007
Available online 4 December 2007
Editor: C.P. Jaupart

Abstract

Debate over the mechanism of accretion of the lower oceanic crust has centered around the gabbro glacier and the sheeted sills models. The thermal profile of the crust, specifically the roles of hydrothermal circulation and cooling rate, is a key component in distinguishing between these two models. Results of this study show no systematic variation of cooling rate with depth in the lower crust of the Khafifah section in the Wadi Tayin massif of the Oman ophiolite. Additionally, very high rates recorded near the base of the crust suggest that hydrothermal circulation plays an important role in the removal of heat throughout the crust. While the conclusions presented here do not rule out the possibility of accretion by gabbro glacier, they do contradict the initial tenet of the gabbro glacier model – convective heat loss by hydrothermal circulation *can* penetrate to Moho depths and crystallization is *not*, by necessity, constrained to the upper crust. On the basis of these results it can be concluded that the sheeted sills model is a thermally viable mechanism for accretion of oceanic lower crust.
© 2007 Elsevier B.V. All rights reserved.

Keywords: calcium; olivine; oman; hydrothermal; cooling; crust

1. Introduction

Mid-ocean ridges serve as the primary locus for heat and mass transfer between the Earth's interior and the hydrosphere. Yet due to the complexity of direct sampling, the first-order processes that control the igneous accretion and hydrothermal cooling of the lower oceanic crust remain poorly understood. Currently, the debate over the processes of accretion of the lower crust at mid oceanic spreading centers is centered on two end-member models: the gabbro glacier model and the sheeted sills model (Fig. 1). The gabbro glacier model proposes that the oceanic crust below the sheeted dikes is formed via crystallization in a single melt lens located at the base of the sheeted dike section (e.g., Nicolas et al., 1988; Henstock et al., 1993; Phipps Morgan and Chen, 1993; Quick and Denlinger, 1993). Conversely, in the sheeted sills model, the lower crust forms in several melt lenses at different depths and crystallizes *in situ* (Korenaga and Kelemen, 1997; Kelemen et al., 1997; Kelemen and Aharonov, 1998). In fact, all papers advocating the sheeted sill mechanism, except that of MacLeod and Yaouancq (2000), have included a small "gabbro glacier," forming the uppermost part of the plutonic crust. Additional intermediate models have been proposed in which sills intrude a gabbro glacier, or in which crust is formed by several gabbro glaciers (Schouten and Denham, 1995; Boudier et al., 1996). Despite these clearly posed alternatives and the range of reasonable, intermediate possibilities, there has been a surprising lack of consensus on which end-member process is most important in forming oceanic lower crust.

One potential means of distinguishing between the gabbro glacier and sheeted sill models is analysis of the cooling rate profile in the lower crust. Quantitative gabbro glacier models incorporate the assumption that hydrothermal circulation does not occur in rocks at more than 600 °C, and that cooling can be modeled as diffusive heat loss with an enhanced diffusivity.

* Corresponding author. Tel.: +1 212 769 5083; fax: +1 212 769 5339.
E-mail address: jvantong@ldeo.columbia.edu (J.A. VanTongeren).

0012-821X/$ - see front matter © 2007 Elsevier B.V. All rights reserved.
doi:10.1016/j.epsl.2007.11.034

Author's personal copy

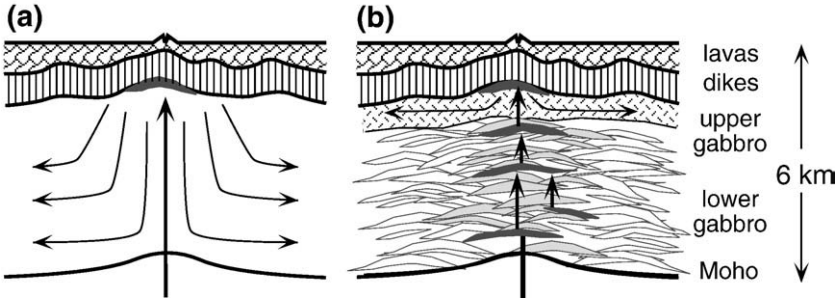

Fig. 1. End-member models for accretion of the oceanic lower crust. a) Gabbro glacier model in which the lower crust is formed via crystallization in a single melt lens situated at the base of the sheeted dikes. b) Sheeted sills model in which the lower crust forms in situ in a series of small sills.

The result of these assumptions is that hydrothermal cooling does not penetrate the lower crust below the shallow melt lens until the crust is far from the ridge axis (Phipps Morgan and Chen, 1993; Chen, 2001). In such models, the most rapid crystallization takes place within a shallow melt lens in the upper 2 km of lower crust. The gabbro glacier model, therefore, predicts a gradual decrease in cooling rate with depth, in which upper gabbro cools by hydrothermal convection and lower gabbro cools much more slowly via conduction. In this case, extensive *in situ* crystallization of lower crust, required by the sheeted sill model, is not thermally possible because the enhanced conductive cooling is insufficient to remove the latent heat of crystallization (Chen, 2001). Alternatively, if active hydrothermal convection extends to the Moho within a few kilometers of the ridge axis, then extensive crystallization could form gabbroic cumulates *in situ* near the base of the crust. Under these circumstances, lower crustal cooling rates will be nearly constant as a function of depth (Cherkaoui et al., 2003; Maclennan et al., 2004).

Articulation of the above cooling rate constraint led to increased interest in explicit modeling of role of hydrothermal convection in the cooling of oceanic lower crust. If near-axis hydrothermal convection in the lower crust is absent or subdued, then the sheeted sill hypothesis is incorrect (Chen, 2001). We believe this reasoning is logical. Conversely, some investigators have suggested that if near-axis hydrothermal convection in the lower crust is vigorous, then the sheeted sill hypothesis must be correct. However, as shown by Buck (2000), a tall, narrow gabbro glacier – just a few kilometers wide – may be present even if hydrothermal convection extends to the Moho within two or three kilometers of the ridge axis. Thus, vigorous, near-axis hydrothermal convection is necessary for the sheeted sill process, but could also be consistent with a modified gabbro glacier model taking place in a narrow "elevator shaft." This said, if vigorous hydrothermal circulation does penetrate to the base of the crust then the absence of substantial igneous crystallization at these depths is unlikely. Additionally, the presence of hydrothermal circulation near the ridge axis in the lower crust eliminates the original justification for the gabbro glacier model, in which crystallization could only happen in a shallow melt lens due to the lack of effective heat transport at depth.

In this study we use the diffusive exchange of calcium and magnesium between olivine and clinopyroxene as a measure of relative cooling rates within lower crustal gabbros in the Wadi Tayin massif of the Oman ophiolite. We present data on the variation of Ca in olivine, and cooling rates, with depth in the crust. We also compare these data with other published data sets for Oman, as well as other gabbroic sections of oceanic crust sampled by drilling, and discuss the results in terms of hydrothermal cooling and igneous accretion of oceanic crust.

2. Background

2.1. The Oman ophiolite

The Oman ophiolite, which formed at a sub-marine spreading center, is an ideal location to study the mechanisms of lower crust accretion and the extent of seawater penetration due to its relatively pristine and easily accessible outcrops. In particular, the Wadi Tayin massif in the southern most section of the Oman ophiolite (Fig. 2) is the best analogue for a paleo-mid ocean ridge because dikes and lavas have a trace element signature similar to that of present day MORB, primitive gabbros lack hornblende and orthopyroxene, and residual mantle peridotites have mineral compositions, particularly spinel Cr/Al ratios, that overlap those for peridotites from modern ridges (e.g., Boudier and Coleman, 1981; Pallister and Knight, 1981; Pallister and Hopson, 1981; Garrido et al., 2001; Hanghoj et al., in preparation).

The Oman lower crust is thought to have formed at an intermediate to fast spreading ridge. Geochronological data on late, tonalite–trondjhemite intrusions are consistent with this range of spreading rates (Tilton et al., 1981). Throughout most of the ophiolite, there is a well-developed layer of gabbroic rocks between sheeted dikes and mantle peridotites (Nicolas et al., 2000), in contrast to that of slow-spreading ridges where lavas are commonly emplaced directly on tectonically exposed peridotite (e.g., Cannat, 1996). Other proposed criteria for estimating spreading rate, such as the presence of plagioclase lherzolites in the mantle section, are unreliable in our opinion.

2.2. Accretion of oceanic lower crust

2.2.1. Evidence in favor of the gabbro glacier model

Geophysical evidence supporting the gabbro glacier model includes seismic reflection images of a shallow melt lens at the base of the sheeted dikes along the East Pacific Rise (EPR)

Author's personal copy

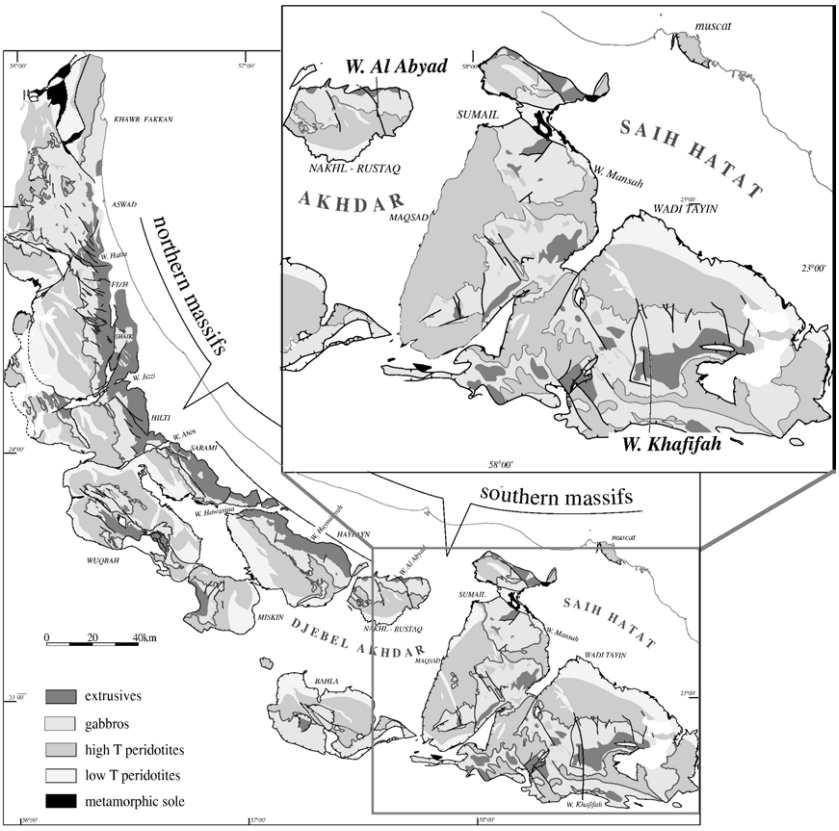

Fig. 2. Map of the Oman ophiolite adapted from Nicolas et al. (2000). Inset shows the sections of Wadi Khafifah (this study) and Wadi Al Abyad (Coogan et al., 2002) in bold lettering. See Garrido et al. (2001) for a map of detailed sample locations and Table 2 for precise UTM coordinates.

(Phipps Morgan and Chen, 1993; Quick and Denlinger, 1993; Hooft et al., 1997; Carbotte et al., 2003). Images of this magma chamber suggest that it is probably less than 100 m thick and either pure melt or partially crystalline mush (Hussenoeder et al., 1996; Collier and Singh, 1997; Singh et al., 1998, 1999). Phipps Morgan and Chen (1993) suggest that crystallization takes place most efficiently at this depth, thereby making the shallow melt lens the dominant supplier of cumulate gabbro for the lower crust.

Petrologic evidence in support of the gabbro glacier model comes from the Oman ophiolite (see Nicolas et al., 1993 and references therein for more detail). First, shear banding in the layered gabbros suggests they were deformed during magmatic flow. Second, lineations and foliations in the gabbros are parallel to the lineation in underlying mantle peridotites, potentially due to viscous coupling between mantle flow and crust. Third, steeply dipping foliations in upper gabbros, compared with shallow dips of layering in lower gabbros, suggests magmatic flow to the sheeted dikes.

2.2.2. Evidence in favor of the sheeted sill model

There is also significant petrologic evidence, however, that is inconsistent with crustal accretion in a gabbro glacier setting (e.g., Korenaga and Kelemen, 1997; Kelemen et al., 1997; Kelemen and Aharonov, 1998; Korenaga and Kelemen, 1998; Garrido et al., 2001). First, delicate, modally graded layering in lower gabbros (e.g., Pallister and Hopson, 1981, Fig. 3d–k) could not survive the shear strain associated with the gabbro glacier model. Second, modally layered gabbro sills in the mantle transition zone (MTZ) formed *in situ*, and not by ductile flow of crystals settling from a large magma chamber. Sills in the MTZ are compositionally and texturally similar to the lower gabbros, and parental to the magmas that formed sheeted dikes and lavas. Since the MTZ sills did not form in a gabbro glacier, and instead crystallized *in situ*, by analogy the lower crustal layered gabbros may have formed in the same manner. Third, the presence of cm-scale chemical variation in the layered gabbros argues against porous melt flow through interconnected porosities within the lower crust, while the gabbro glacier model requires ~20% interconnected porosity for downward ductile flow of a crystal mush from a shallow melt lens (Nicolas, 1992).

In addition, despite the absence of small melt-filled sills in seismic imaging, there is also geophysical data in support of the sheeted sills hypothesis. Most on-axis seismic reflection surveys may only image the shallowest of many small melt lenses; deeper lenses may be shielded from seismic reflections by the uppermost lens. Furthermore, seismic reflection and compliance studies have demonstrated the presence of melt lenses at the base of the crust (Lewis and Garmany, 1982; Crawford et al., 1999; Crawford and Webb, 2002; Nedimovic et al., 2005). From this perspective, the Low Velocity Zone (LVZ) extending from the shallow melt lens to the base of the crust at the EPR (Detrick et al., 1987; Harding et al., 1989; Toomey et al., 1990; Vera et al., 1990; Dunn et al., 2000) could be a region

Author's personal copy

containing many smaller melt lenses (1–100 m) rather than a homogeneous "crystal mush."

2.3. Hydrothermal alteration as a function of depth

In the Oman ophiolite, the crustal section of the Wadi Tayin massif provides a benchmark for studies of hydrothermal alteration of oceanic crust as a function of depth. Gregory and Taylor (1981) showed that lavas, sheeted dikes, and the uppermost gabbros were affected by low-temperature alteration that shifted oxygen isotope ratios to heavier values and $^{87}Sr/^{86}Sr$ closer to seawater values at high water-rock ratios. In the same study, they showed that lower crustal gabbros underwent high-temperature alteration that shifted oxygen to lighter isotope ratios, with less modification of $^{87}Sr/^{86}Sr$ at lower water–rock ratios. These observations are consistent with other ophiolite sections and data from partial oceanic gabbro sections sampled by drilling (e.g., Lanphere et al., 1981; McCulloch et al., 1981; Stakes and Vanko, 1986; Lecuyer and Reynard, 1996; Mevel et al., 1996; Kawahata et al., 2001; Alt and Bach, 2006).

Recently, there has been an emphasis on anisotropic distribution of fluid flow and alteration in the lower crust. High-temperature hydrothermal veins record much larger shifts to lighter oxygen isotopes and higher $^{87}Sr/^{86}Sr$ in the lower crust (Bosch et al., 2004; Coogan et al., 2006), indicating the presence of high flux channels for focused flow during high-temperature hydrothermal circulation. Systems of sub-millimeter microcracks that penetrate to the Moho in Oman lower gabbros have been described by numerous workers (Nicolas et al., 1988; Nehlig, 1994; Nicolas et al., 2003). These microcracks are thought to be interconnected and the cracking events episodic, presumably due to thermal contraction caused by the cooling of the gabbro. Because heat diffuses much more rapidly than chemical components, a few zones with focused fluid flow could drive rapid cooling in large domains within oceanic lower crust. Amphibolite facies mineral assemblages, as well as oxygen and strontium isotopes, suggest that these cracks formed at very high temperatures (900-1000 °C; Bosch et al., 2004).

The modeling study of Cherkaoui et al. (2003) showed that oceanic lower crust may cool efficiently via vigorous hydrothermal convection at permeabilities $\geq 2\times10^{-14}$ m^2. In this case, near-axis isotherms in the lower crust are essentially vertical from the base of the sheeted dikes to the Moho, implying uniform cooling throughout the lower crust. Dunn et al. (2000) presented an interpretation of lower crustal seismic data for the EPR in which seismic velocity is slowest beneath the ridge axis, and contours of seismic velocity are nearly vertical. Cherkaoui et al. and Dunn et al. interpreted these results to indicate that vigorous hydrothermal cooling extends to the base of the crust along the EPR.

2.4. Cooling rates as a function of depth

Ultimately, the correct model for oceanic crustal accretion and the influence of hydrothermal cooling in the lower crust must agree not only with petrologic and geophysical observations from spreading centers, but also with data on the thermal profile of the lower crust. The latter can be quantified based on cooling rates of the cumulate gabbros.

Two previous studies have been conducted on the variation of cooling rate as a function of depth in the lower crust of the Oman ophiolite. Garrido et al. (2001) measured plagioclase crystal size distribution (CSD) through the Khafifah section of the Wadi Tayin massif, and found evidence for a transition from conduction dominated cooling in the lower gabbros (below 1500 m) to a hydrothermally dominated cooling profile in the upper gabbros (above 2500 m). Garrido et al. (2001) concluded that their data were consistent with the sheeted sill model of emplacement. Coogan et al. (2002) calculated cooling rates using Ca in olivine in the Wadi Abyad massif, and reported a gradual decrease in cooling rate with increasing depth in the section. On the basis of these results they argued in favor of the gabbro glacier model. The work presented here extends the technique of Coogan et al. (2002) to the sample suite from the Khafifah section in the Wadi Tayin massif of the Oman ophiolite, previously studied by Garrido et al. (2001).

3. Methods

3.1. Samples

Samples were taken from the lower gabbro section in the Wadi Tayin massif of the Oman ophiolite (See Garrido et al. (2001) for sample locations and descriptions). All thin sections were previously analyzed by Garrido et al. (2001) in a study of plagioclase CSDs. Olivine crystals for this study were selected according to two criteria: crystal freshness and crystal shape. Sub-spherical olivines, with aspect ratios less than 3.0, were selected to maximize the likelihood of analyzing the true center of the crystal.

3.2. Electron microprobe analyses

High precision electron microprobe analyses were conducted at The American Museum of Natural History on a Cameca Sx100 microprobe. A 100 nA beam current, and 15 kV were used for 600 s on the peak, and 300 s on each background for Ca in olivine. In a previous Ca in olivine study, Coogan et al. (2002) used a 200 nA beam, 15 kV, and counting times of 600 s peak and 300 s background and reported counting statistics of ±2% relative at 1 σ. Mantle Ca in olivine measured by M. Braun (2004) used a 100 nA beam, 15 kV, and 240 s on peak and 180 s on background for precision of ±1.5% relative at 1 σ. Analytical conditions for this study were chosen based on these results. Standards were reproduced to better than ±5% relative (1 σ) over a range of concentrations between 100 and 700 ppm (Table 1a). Crucially, we checked for inter-laboratory bias by analyzing Ca in olivine in samples loaned to us by L. A. Coogan, and discovered no significant difference between our analyses and his earlier results. Repeat analyses on two olivine grains with different Ca concentrations yielded an accuracy (with respect to L.A. Coogan's analyses) of ±~1.5% relative, and ±0.9% relative at 1 σ, respectively. Precision of these

Author's personal copy

Table 1a
Error statistics on olivine standards

Standards					
Standard	*n*	Mean Ca (ppm)	Standard deviation	Counting error (ppm)	% relative
SC_Oliv	43	716.04	12.05	4.68	1.68
OL_Que	25	260.66	9.47	1.84	3.63
OL174.1	15	99.07	5.56	0.68	5.61

Table 1b
Statistics on inter-lab comparison

Interlab comparison					
	Average Ca (ppm)	Standard deviation (ppm)	Coogan reported value (ppm)	% rel error	% error (ppm)
Grain 1; $n=8$	319.40	5.60	314.44	1.58	5.04
Grain 2; $n=7$	1558.36	18.63	1572.21	0.88	13.73

analyses was well within the standard deviation of the accuracy (Table 1b).

All olivine grains were analyzed in both core and rim. Closely spaced traverses through each olivine were made where possible in order to determine a diffusion profile. An average of four olivine grains were analyzed per thin section resulting in an average of thirteen analyses per thin section.

3.3. Calculation of closure temperature and cooling rate

Temperatures are calculated using the experimentally derived Ca-in-olivine thermometer of Kohler and Brey (1990).

$$T_c = \frac{42.5P + 5792}{-\ln\left(D_{\mathrm{Ca}}^{\mathrm{ol/cpx}}\right) - 1.25} \quad (1)$$

Pressure is assumed to be 200 MPa. $D_{Ca}^{ol/cpx}$ is the distribution coefficient of Ca between olivine and clinopyroxene. Cooling rates (dT/dt) are calculated following the equations of Dodson (1973).

$$dT/dt = \frac{-\mathrm{RT}_c^2 \mathrm{AD}_o}{\mathrm{Ea}^2 \exp(E/\mathrm{RT}_c)}. \quad (2)$$

A is a dimensionless number assigned for crystal shape (e.g. 55 for a sphere, assumed throughout the calculations); a is the diffusion length, here defined as the crystal radius (or the minimum core to rim diffusion length in crystals with aspect ratios >1); D_o is the pre-exponential diffusion constant; and E is the activation energy associated with the specified D_o and the axis of maximum diffusivity.

3.4. Potential complications in the measurement of cooling rate from Ca in olivine

3.4.1. Diffusivity of Ca in olivine

The choice of pre-exponential diffusion constant (D_o) for Ca in olivine has been the subject of debate since the first study published by Morioka (1981). In fact, cooling rates calculated based on the D_o and E of Jurewicz and Watson (1988) are shown to be markedly different than those calculated using results reported by Stahl et al. (1998) (e.g., Coogan et al., 2002). Fig. 3 demonstrates the current range in published values for D_o as a function of temperature. For this reason, until D_o and E are known precisely, calculated cooling rates based on Ca diffusion in olivine are best considered as relative estimates (Coogan et al., 2005). We place most confidence in the experimentally calibrated diffusivities of Coogan et al. (2005), due to their calibration over a wide range of temperature (1500–900 °C) and forsterite content (Fo_{100}–Fo_{83}).

3.4.2. Dependence of calcium diffusivity on olivine forsterite content

It has been proposed that increased Fe concentration leads to increased diffusivity of Ca in olivine (Roeder, 1974; Longhi et al., 1978; Jurewicz and Watson, 1988; Libourel, 1999). Coogan et al. (2005) suggest that there is no correlation between decreased forsterite content and faster Ca diffusivity. Data from our study show a small correlation ($R^2=0.14$) between Fo and Ca content. Thus, Ca concentration and cooling rate values reported throughout this study are not corrected for any possible dependence of diffusivity on Fe content of olivine.

3.4.3. Stereological effects and crystallographic orientation in thin section

One complication in interpreting Ca content in olivine cores arises from uncertainty associated with crystal shape in three

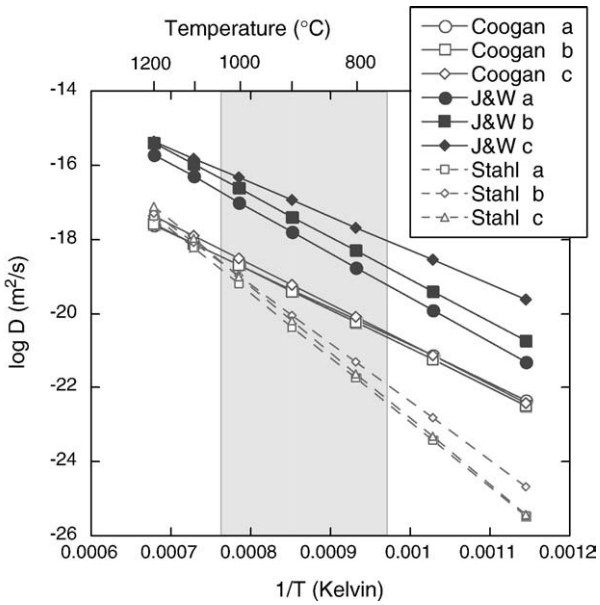

Fig. 3. Experimentally determined pre-exponential diffusion constants (D_o) for Ca in olivine. J&W=Jurewicz and Watson (1988); Stahl=Stahl et al. (1998); Coogan=Coogan et al. (2005). a, b, and c=a, b, and c crystallographic axes. Most confidence is placed in the results of Coogan et al. (2005) because of their calibration over a wide range of temperature and olivine forsterite content. Calculations of cooling rate reported throughout this study use the D_o and E of the Coogan et al. (2005) c-axis. Gray shaded area denotes the temperature interval of interest in this study.

Author's personal copy

Table 2
Results of detailed electron microprobe analyses of Ca in olivine cores

Sample ID	UTM (E)	UTM (N)	Depth (m)	Grain radius (mm)	Ca (ppm)	T (°C)	Cooling Rate (°C/Yr)
OM97-67a-2-3	065 03 33	25 35 082	46	0.10	260.1	795.01	5.73E-02
OM97-67a-3-2			46	0.52	309.6	830.86	4.82E-03
OM97-45-1.1	064 74 95	25 35 235	162	0.16	281.6	811.99	3.32E-02
OM97-45-2.2			162	0.20	208.4	755.99	5.49E-03
OM97-45-3.1			162	0.18	163.9	714.86	2.28E-03
OM97-45-4.4			162	0.20	323.8	842.99	4.26E-02
OM97-52-1.3	064 74 95	25 35 235	525	0.12	350.9	864.59	1.88E-01
OM97-52-2.2			525	0.16	355.3	866.99	1.11E-01
OM97-52-3.1			525	0.20	390.5	889.32	1.12E-01
OM97-52-4.1			525	0.14	382.8	885.10	2.11E-01
OM97-59a-1-1	064 74 95	25 35 235	640	0.20	672	1018.95	1.19E+00
OM97-59a-2-2			640	0.20	706.8	1034.63	1.54E+00
OM97-59a-3-1			640	0.30	571.1	973.77	2.45E-01
OM97-59a-4-2			640	0.44	619.6	996.83	1.70E-01
OM97-75-1-3	064 69 47	25 34 217	719	0.20	639.3	1010.42	1.03E+00
OM97-75-2-1			719	0.34	603	993.78	2.70E-01
OM97-75-4-2			719	0.18	521.8	955.35	4.90E-01
OM99-40-1-1	064 67 87	25 33 534	961	0.40	634.3	1005.52	2.38E-01
OM99-40-3			961	0.36	660.1	1018.38	3.64E-01
OM99-40-4			961	0.50	663.8	1018.09	1.88E-01
OM99-40-4b			961	0.50	636.3	1005.28	1.52E-01
OM99-44-1	064 61 24	25 33 154	1253	0.18	618.1	998.90	1.05E+00
OM99-44-2			1253	0.40	673	1023.62	3.21E-01
OM99-44-3			1253	0.28	643.7	1007.90	5.05E-01
OM99-44-4			1253	0.40	639	1009.35	2.54E-01
OM99-47-1	064 72 13	25 32 471	1392	0.36	475.3	925.07	6.98E-02
OM99-47-2			1392	0.26	477.2	926.48	1.37E-01
OM99-47-3			1392	0.60	494.1	933.45	2.94E-02
OM99-47-4			1392	0.38	491.4	934.64	7.50E-02
OM99-47-5			1392	0.46	467.5	919.69	3.86E-02
OM99-51-2	064 73 95	25 32 127	1535	0.34	319.6	829.24	1.09E-02
OM99-51-3			1535	0.36	321.9	830.52	9.99E-03
OM99-51-4			1535	0.28	290.9	810.44	1.05E-02
OM99-51-5			1535	0.48	364.1	857.18	1.00E-02
OM97-89-1.4	064 74 33	25 31 650	1793	0.32	379.1	875.35	3.30E-02
OM97-89-2.2			1793	0.46	351.2	858.57	1.13E-02
OM97-89-3.2			1793	0.24	300.4	824.14	1.95E-02
OM97-89-4.1			1793	0.32	323.4	840.38	1.57E-02
OM97-94a-1-1	064 76 01	25 31 070	2011	0.54	514.7	947.93	4.75E-02
OM97-94a-2-4			2011	0.66	467.4	923.77	2.03E-02
OM97-94a-3-1			2011	0.34	345.9	855.26	1.92E-02
OM97-94a-4-1			2011	0.40	414.1	896.08	3.22E-02
OM97-200-1-1	064 95 66	25 30 116	2181	0.22	587.9	985.73	5.61E-01
OM97-200-2-1			2181	0.26	601.3	991.86	4.47E-01
OM97-200-4-1			2181	0.28	516.6	947.94	1.77E-01
OM97-99-1.1	064 91 81	25 30 214	2193	0.12	407.7	893.96	3.43E-01
OM97-99-2.2			2193	0.16	417.9	899.76	2.16E-01
OM97-99-3.2			2193	0.24	510.7	947.59	2.39E-01
OM97-97a-1-2	064 85 61	25 30 315	2257	0.36	591.7	1003.00	2.82E-01
OM97-97a-2-1			2257	0.48	603.5	1007.38	1.71E-01
OM97-97a-3-3			2257	0.50	458.9	936.68	4.50E-02
OM97-95-1.1	064 76 32	25 30 434	2303	0.30	411.3	888.45	4.91E-02
OM97-95-2.1			2303	0.30	402.9	884.08	4.49E-02
OM97-95-3.3			2303	0.14	330.8	840.92	8.31E-02
OM97-95-4.1			2303	0.22	366.8	863.83	5.50E-02
OM97-102-1-1	064 95 07	25 29 684	2369	0.24	383	878.18	6.22E-02
OM97-102-2-1			2369	0.18	315.6	835.88	4.50E-02
OM97-102-3-2			2369	0.24	277.6	811.23	1.45E-02
OM97-102-4-3			2369	0.16	333.7	848.03	7.42E-02
OM97-104-1-2	064 95 74	25 28 329	2999	0.26	293.8	820.41	1.53E-02
OM97-104-2-2			2999	0.14	360.4	863.79	1.36E-01
OM97-104-3-1			2999	0.22	285.7	815.95	1.93E-02
OM97-104-4-2			2999	0.30	287.4	815.95	1.04E-02

Author's personal copy

Table 2 (*continued*)

Sample ID	UTM (E)	UTM (N)	Depth (m)	Grain radius (mm)	Ca (ppm)	T (°C)	Cooling Rate (°C/Yr)
OM97-104-4-2			2999	0.30	287.4	815.95	1.04E-02
OM97-106-2.2	064 91 06	25 27 817	3260	0.16	497.1	953.74	6.02E-01
OM97-106-3.1c			3260	0.12	469.6	938.23	8.05E-01
OM97-106-4.1			3260	0.22	447.4	927.13	1.94E-01
OM97-204-1.2	064 84 67	25 27 222	3573	0.18	246.9	784.08	1.36E-02
OM97-204-2.3			3573	0.11	265.1	796.75	4.93E-02
OM97-204-3.4			3573	0.18	281.9	808.47	2.42E-02
OM97-204-4.4			3573	0.14	259.9	789.91	2.59E-02
OM97-111-1.4	064 83 73	25 27 198	3594	0.34	429.2	903.92	5.20E-02
OM97-111-2.3			3594	0.24	310.2	831.78	2.31E-02
OM97-111-3.1			3594	0.20	268.7	803.07	1.73E-02
OM97-111-4.1			3594	0.24	371.5	869.92	5.25E-02
OM97-110-1-2	064 83 48	25 27 124	3627	0.52	411.4	895.67	1.89E-02
OM97-110-2-5			3627	0.48	395.2	884.94	1.79E-02
OM97-110-3-1			3627	0.70	343.1	854.51	4.46E-03
OM97-110-4-2			3627	0.40	431.3	906.22	3.93E-02
OM97-110-5-1			3627	0.34	321.6	840.62	1.40E-02
OM97-108-1-2	064 82 55	25 271 37	3632	0.44	321.8	835.63	7.49E-03
OM97-108-2-2			3632	0.34	331.7	841.84	1.44E-02
OM97-108-3-1			3632	0.24	372.2	868.05	5.04E-02
OM97-108-5-1			3632	0.24	321.1	835.13	2.49E-02
OM97-112-1.1	064 82 74	25 26 987	3691	0.44	439.6	906.70	3.28E-02
OM97-112-2.2			3691	0.40	431.4	901.65	3.59E-02
OM97-112-3.1			3691	0.48	351	854.67	9.51E-03

Calculations of closure temperature (T_c) and cooling rate are discussed in the text. All electron microprobe data is available in Supplementary Data Table 1.

dimensions. It is difficult to determine whether or not thin sections pass close to the core of a given crystal. As mentioned previously, olivines analyzed for this study were selected based on their shape, and only grains having aspect ratios less than 3.0 were analyzed. Despite this, we cannot rule out the possibility that the thin section is close to a grain edge in the third dimension. In order to identify those grains in which the section was not cut through the center, cores and rims of all grains were analyzed. Profiles from rim to rim were measured through one or more olivine grains per section in order to identify core to rim variation without X-ray fluorescence effects (see Section 3.4.5). In cases where we analyzed apparent olivine cores that were close to a grain edge in the third dimension, the effect will be to underestimate actual Ca concentration in olivine cores, reducing the estimated cooling rate (Ehlers et al., 1994). In order to minimize this potential bias, only the highest measured Ca values from each crystal core were used in the calculation of closure temperature and cooling rate. This assumes that the highest Ca value is closest to the true core value and therefore provides the most accurate cooling rate estimate.

3.4.4. Secondary X-ray fluorescence

Secondary X-ray fluorescence can be a problem in measurement of Ca in olivine adjacent to clinopyroxene. Dalton and Lane (1996) found that significant biases existed in measurements made 3 μm from the contact with clinopyroxene in Fe-free olivine, but that fluorescence length increases with increasing Fe content of olivine upwards from 50 μm in Fo_{90} olivine. For this reason, we used only core Ca in olivine measured more than 50 μm from crystal edges in thin section.

4. Results

Results of electron microprobe analyses of Ca in olivine are given in Table 2 and plotted versus depth in the crustal section in Fig. 4a. In addition to our new data, samples plotted at 3 km below the base of the crust are precise mantle olivine analyses from M. Braun (2004). These mantle olivines are in harzburgite with exsolved pyroxene crystals, and two pyroxene thermometry is in overall agreement with olivine–clinopyroxene Ca exchange temperatures (Hanghoj et al., in preparation), indicating that olivine, orthopyroxene and clinopyroxene approached cation exchange equilibrium during cooling. As predicted, Fig. 4a indicates that Ca in olivine is consistently higher in the crustal section than in residual peridotites. This may reflect a slower cooling rate at these depths. Calculated Ca-in-olivine closure temperatures for lower crustal gabbros are shown in Fig. 4b, and follow approximately the same trend as the Ca data shown in Fig. 4a. Error bars shown in Fig. 4a represent one standard deviation from the mean of the highest Ca value in each olivine grain analyzed per depth section. Likewise, error bars in Fig. 4b represent one standard deviation from the mean of the highest closure temperatures recorded in each olivine grain per section.

Fig. 4c shows the variation in cooling rate with depth in the section. Values represent the average of the cooling rates calculated from the highest Ca concentration in the cores of each grain (approximately 4 grains per depth section were averaged). Because grain size can vary greatly, while core Ca content varies less drastically, the slowest cooling rates calculated from small grains are faster than cooling rates associated with large grains and have larger errors associated with them. The error

Author's personal copy

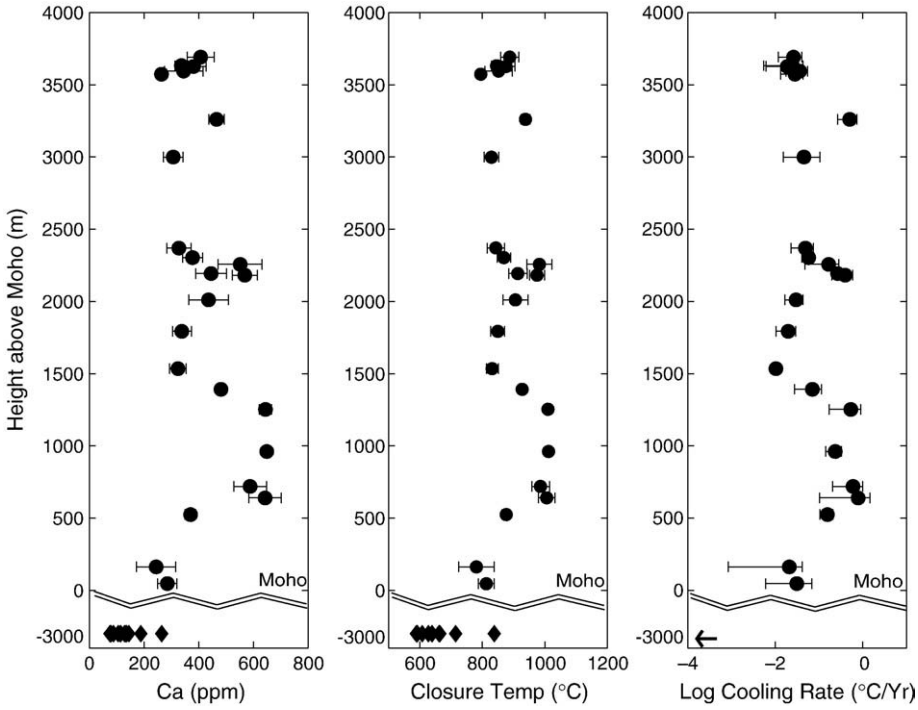

Fig. 4. Results of Ca in olivine from detailed electron microprobe analysis. a) average Ca concentration in olivine cores from each depth section. b) average calculated closure temperature (T_c). c) average calculated cooling rate from Ca in olivine analyses. Cooling rates are calculated using the D_o and E of Coogan et al. (2005). See text for discussion of error bars. Samples plotting below the Moho are precise mantle analyses taken from M. Braun (PhD thesis). The arrow in plot c is shown in place of mantle cooling rates plotting from 10^{-7} to 10^{-14} °C/year.

bars shown in Fig. 4c represent one standard deviation from the mean cooling rate. We feel this is the most robust estimate of uncertainty associated with these calculations because it incorporates all possible non-systematic errors, such as those associated with the measurement of Ca content as well as grain size and cut of the thin section plane. These errors should be considered as maximum values and overestimate real uncertainty in most cases.

Cooling rates for mantle samples are calculated using a uniform grain size of 1 mm because grain size was not recorded during analyses from Braun (2004). Mantle samples have cooling rates at least seven orders of magnitude slower than that of the overlying crust (Fig. 4c).

In contrast to the results of Coogan et al. (2002), our data show no systematic trend of Ca in olivine, Ca-in-olivine closure temperature, or cooling rate with depth. Also, in general, we measured higher Ca in olivine than Coogan et al. (2002) at most depths, for crystals with the approximately the same grain size. Fig. 5 illustrates the influence of grain size on Ca in olivine. Data points represent individual analyses of the highest T_c

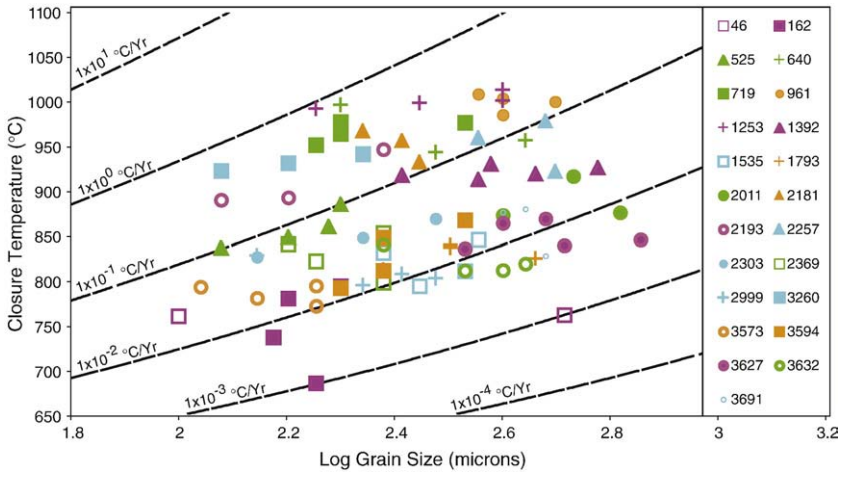

Fig. 5. The influence of grain size on cooling rate. Dashed black lines represent uniform cooling rate calculated from grain size and closure temperature. Numbers at right correspond to depths (in meters) within the Khafifah section. Symbols plot closure temperature calculated from the highest Ca concentration in a single grain. Similar to the findings of Ozawa (1984), olivine grain size has a large effect on the calculation of cooling rate. Note log grain size plotted on a linear scale.

Author's personal copy

(calculated from highest Ca content) measured in the cores of each grain analyzed. Solid black contours delineate cooling rate. Similar to Ozawa (Ozawa, 1984, Figs. 9–14), for several of our samples olivine analyses lie along contours of constant cooling rate. It can be concluded that core Ca is approximated well by our analytical procedure despite the potential biases mentioned previously (Section 3.4).

5. Discussion

The absence of systematic variation in cooling rate with depth recorded in the Wadi Tayin crustal section of the Oman ophiolite suggests that the gabbros cooled at approximately the same rate throughout the lower crust (Fig. 4). Lower crustal gabbros with faster cooling rates than those of gabbros near the base of the sheeted dikes, may have been intruded off-axis where host rock had already cooled significantly (MacLeod and Yaouancq, 2000). Since oceanic crust shows no appreciable increase in thickness more than one km off axis (Vera et al., 1990; Singh et al., 2006), these off-axis intrusions must have been within one km of the ridge axis, and thus rapid cooling of host rocks is required by these data. As mentioned previously (Section 1), in order to cool the lower crust at a uniform rate from the Moho to the sheeted dikes, hydrothermal circulation must be active throughout the crust within one or two km of the ridge axis. Results from this study are therefore consistent with vigorous hydrothermal cooling to Moho depths within one or two km of the ridge axis.

5.1. Comparison with previous cooling rate studies in the Oman ophiolite

5.1.1. Comparison with previous Ca in olivine results

Our results are different than a previous study of Ca in olivine in the lower crust in the Wadi Abyad section of the Nakhl massif of the Oman ophiolite by Coogan et al. (2002). Fig. 6a shows data from this study compared to the data of Coogan et al. (2002). To directly compare the two datasets, cooling rates for the Coogan et al. data were calculated with the pre-exponential diffusion constant (D_o) and corresponding activation energy (E) of Coogan et al. (2005), assigning the same crustal thickness to both sections, and using a constant value of 55 for the geometric parameter A in the cooling rate calculation (Eq. (2), Section 3.3). The cooling rate calculations of Coogan et al. (2002) required a variable geometric parameter, A. Our study does not require this variable because only core analyses are included in our calculation of cooling rate, and A can be considered constant. Using a constant A value of 55 has no effect on the trend of decreasing cooling rate with increasing depth in the data of Coogan et al. (2002) (Fig. 6b).

Our data suggest that the Wadi Tayin massif cooled approximately one order of magnitude more slowly than the Wadi Abyad section for the shallowest gabbros, at the base of the sheeted dikes, and over two orders of magnitude faster than the Wadi Abyad section at the Moho. Also, we see no systematic trend of decreasing cooling rate with increasing depth below the paleo-seafloor, unlike Coogan et al. (2002).

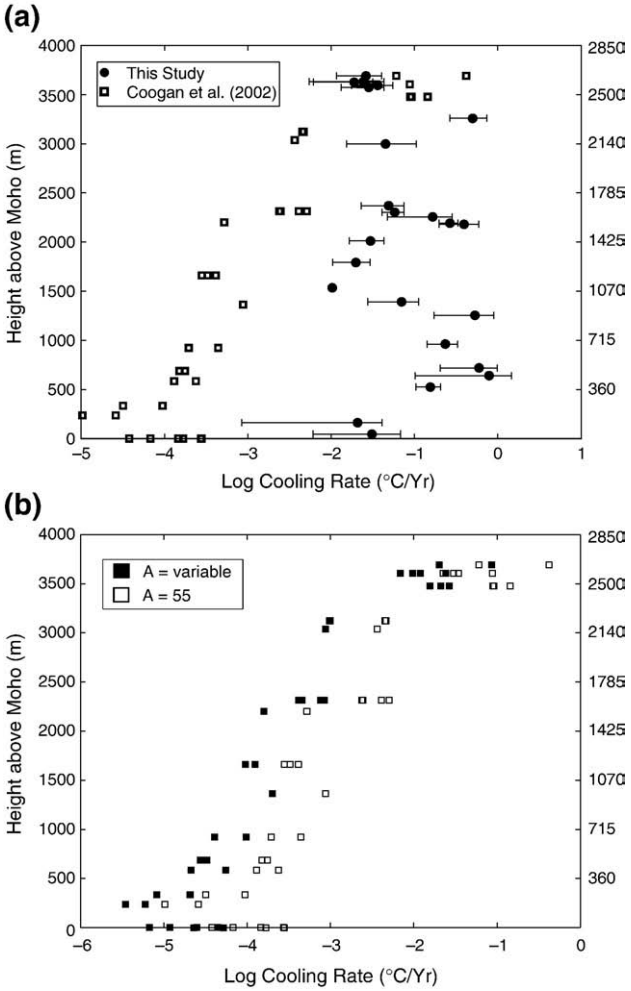

Fig. 6. a) Comparison of cooling rates from Ca in olivine from the Oman ophiolite. Solid circles are cooling rate data from the average of the highest core Ca determined from this study; open squares are cooling rate data from Coogan et al. (2002). Depths reported on the left-side y-axis are those of this study, and depths on the right-side y-axis are those of the Coogan et al. data. For accurate comparison the data of Coogan et al. (2002) have been recalculated using the D_o of Coogan et al. (2005) and a constant geometric parameter, $A=55$. Although the data presented here is the reported Bulk Ca Content from Coogan et al. (2002; Table 1) and not the highest core Ca, according to Coogan et al. (2002, Fig. 7a caption) this "should not shift the data noticeably." b) The effect of variable geometric parameter, A, in the calculation of cooling rate. Solid squares are cooling rates calculated from Coogan et al. (2002) using a variable geometric parameter, A. Open squares are cooling rates calculated from Coogan et al. (2002) using a constant value of 55 for A. This recalculation does not seem to have an effect on the overall trend seen in the data and all data from Coogan et al. (2002) reported in this study are calculated using a constant $A=55$.

Analytical methods and data analysis presented in this study are equivalent to those of Coogan et al. (2002), and we have reproduced their analyses of some samples. Therefore, the differences between the two datasets must be due to differences between the two crustal sections. Here we present three possibilities for the discrepancy between these two datasets.

(1) The Wadi Abyad section is part of the Nakhl–Rustaq massif, from the central part of the Oman ophiolite (Fig. 2). The central and northern sections of the Oman

Author's personal copy

ophiolite have trace element signatures indicative of a subduction-component (Pearce et al., 1981; Alabaster et al., 1982; Lachize et al., 1996; Arai et al., 2006; Tamura and Arai, 2006). It is unclear, however, what influence a subduction component may have on cooling rates in the lower crust at intermediate-fast spreading ridges.

(2) The lower crust of the Wadi Abyad section is 2.6 km thick, as compared to a thickness of 3.7 km in Wadi Tayin. Phipps Morgan and Chen (1993) proposed that thinner crust implies a smaller melt flux and therefore a deeper magma chamber. According to Phipps Morgan and Chen (1993; Figs. 4 & 5) a thinner crust would cool more quickly than a thicker crust with a shallower magma chamber. The difference in thermal regime associated with crustal thickness and magma chamber depth, therefore, would be opposite to that which is seen from Ca in olivine results presented in Fig. 4.

(3) Magmatism in the central and northern massifs is polygenetic, with a later suite of plutonic rocks intruding older lower crustal gabbros (e.g., Smewing, 1981; Juteau et al., 1988a,b). In this context, it is relevant that there is a major swarm of gabbronorite dikes intruding the shallow mantle section of the Nahkl massif, just a few kilometers from the base of the Wadi Abyad crustal section (e.g., Nicolas et al., 2000; Fig. 5). In particular, we think it is possible that reheating and retrograde metamorphism due polygenetic crustal formation in this region may have contributed to anomalously slow cooling rates at the base of the Wadi Abyad crustal section.

Some combination of these factors may account for the difference between our results and those of Coogan et al. (2002). In any case, because the composition and crustal thickness of the Wadi Tayin massif of the Oman ophiolite is most similar to composition and crustal thickness at active mid-ocean ridges, we suggest that more confidence should be placed in the results presented from the Wadi Tayin massif (this study) as an analogue for mid-ocean ridge processes.

5.1.2. Comparison with plagioclase crystal size distributions

The results of Garrido et al. (2001) on the same sample suite used in this study do not show any significant correlation with the findings of this study. Using data on crystal size distributions (CSDs), Garrido et al. inferred a transition from rapid to gradual cooling rates of the lower gabbros at approximately 1500 m above the Moho. More confidence must be placed in the cooling rates based on Ca in olivine presented here for two reasons. First, cooling rates determined by plagioclase CSDs were not quantified by Garrido et al. because prior calibrations of CSD versus cooling rate were made for widely separated crystals in a large volume of magma, whereas Oman gabbros solidified 100%, with impinging crystals. Thus, the CSD data are simply a qualitative reflection of the cooling rate and thermal profile. Second, significant factors other than cooling rate, such as variable amounts of second phase pinning, may cause variation of CSDs in holocrystalline rocks that is independent of cooling rate.

5.2. Comparison with model results

5.2.1. Numerical Models

Numerical calculations by Maclennan et al. (2004, 2005) show the thermal regime and surface heat flow for gabbro glacier and sheeted sill models. Intrusion of melt was assumed to take place over a lateral range of 1 km (half width), and the distribution of melt and location of crystallization was allowed to vary. Hydrothermal circulation was treated as a series of heat sinks following the method of Morton and Sleep (1985).

Similarly, numerical models by Cherkaoui et al. (2003) show thermal gradients and fluid flux fields in the lower crust. In these models, however, all lower crust gabbros were assumed to crystallize in situ at the final depth of emplacement, and permeability was varied in order to assess the ability of hydrothermal circulation to efficiently cool the crust. Cherkaoui et al. (2003) concluded on the basis of these models that hydrothermal circulation is very efficient at cooling the lower crust at crustal permeabilities of 2×10^{-14} m^2 and greater. Under these conditions the sheeted sill model of emplacement is thermally viable. While permeability in the lower crust measured from boreholes is typically approximately 10^{-17} except near faults and shear zones (Fisher, 1998), it is likely that higher permeabilities exist during rapid thermal contraction (Cherkaoui et al., 2003; Nicolas et al., 2003; Bosch et al., 2004). Rapid circulation in focused, high permeability zones may be sufficient to cool substantial portions of the lower crust.

Cooling rates for all model outputs of Cherkaoui et al. (2003; Fig. 10) (with the exception of the 7×10^{-17} model run discussed below) were calculated by digitizing the figure and measuring the off-axis distance from the 1200 °C isotherm to the 700 °C isotherm. The resulting °C/km was then multiplied by the half-spreading rate used in the model (50 mm/yr) resulting in °C/yr. The lowest permeability model (7×10^{-17}) was calculated differently because the 700 °C isotherm does not reach Moho depths (6 km in Fig. 10 of Cherkaoui et al., 2003) within the bounds provided by the figure. In this case, the determination of °C/km was again made by digitizing the model output, but the isotherms were then numerically fitted and extrapolated off-axis in order to obtain an accurate estimate of °C/km. The estimate of cooling rate in this calculation is not significantly affected by the choice of temperature interval (See Supplementary Fig. 1). The 700 °C isotherm was chosen as an end point because all Ca in olivine closure temperatures calculated in this study (Table 2) are above 700 °C.

Ca in olivine cooling rate data from this study fit well within the predicted cooling rates from both numerical studies (Fig. 7). A lower bound on cooling rates in the lower crust is provided by the Maclennan et al. (2005) conduction-only model, as well as the $k_o=7\times10^{-17}$ simulation of Cherkaoui et al. (2003). Cooling rates from this study are systematically higher than the lower bounds, and are thus consistent with significant hydrothermal cooling of the lower oceanic crust. Upper bounds for cooling rate in Fig. 7 are calculated from the $k_o=2\times10^{-14}$ simulation of Cherkaoui et al. (2003) in which high permeability and rapid hydrothermal convection extends to the base of the crust. These upper bounds on cooling rate are exceeded by several of our

Author's personal copy

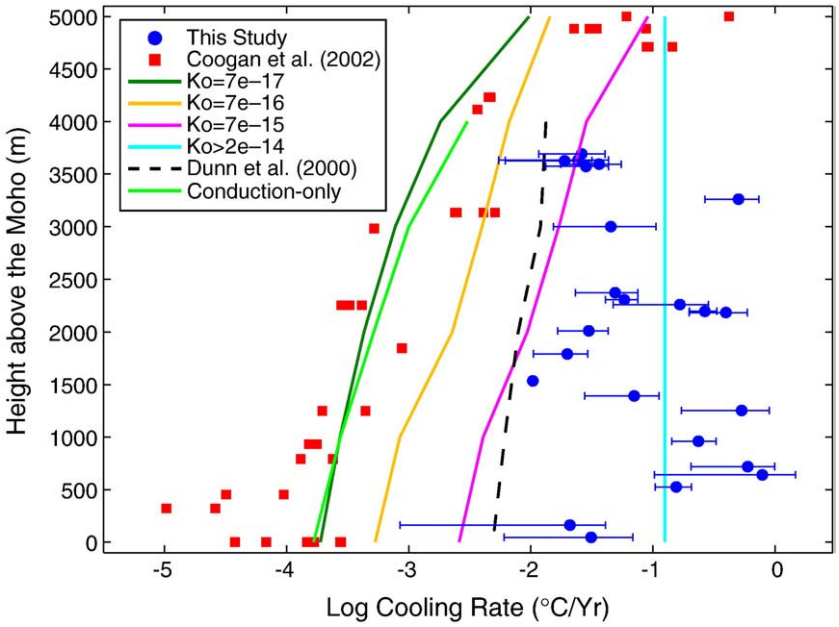

Fig. 7. Comparison of Ca in olivine cooling rates with numerical and geophysical models. Results for cooling rates in the lower crust from the models of Cherkaoui et al. (2003) are presented in terms of varying crustal permeability (k_o) and therefore capacity for hydrothermal circulation. Lower bounds on the cooling rate are given by $k_o = 7\times10^{-17}$ from Cherkaoui et al. (2003, Fig. 10) as well as a model of heat loss by conduction only (Conduction-only) from Maclennan et al. (2005) using the methods of Maclennan et al. (2004). Upper bounds on the cooling rate in the lower crust are given by $k_o = 2\times10^{-14}$ model of Cherkaoui et al. (2003, Fig. 10). Dashed black line is the cooling rate determined from isotherms by Dunn et al. (2000). Data from this study (solid blue circles) fit well within the bounds of numerical and geophysical models, in contrast to the data from Coogan et al. (2002) (solid red squares), which fall outside the lower bounds for cooling. See the text for calculation of cooling rates from model outputs.

data at various points throughout the gabbro section. This may be due to the intrusion of sills slightly off-axis, into colder host rock. In the data of Coogan et al. (2002), gabbros in the lower half of the gabbroic section apparently cooled more slowly than the lower bound limit of conduction alone (Fig. 7). Perhaps, as suggested above, this is due to late reheating and retrograde metamorphism at the base of the Wadi Abyad section, yielding an apparent cooling rate that is slower than would be possible for crust formed in a single spreading-ridge event. Alternatively, perhaps the diffusivity of Ca in olivine used in our calculations is incorrect, in which case all cooling rates would be systematically affected. The range of cooling rates, however, would not be affected by calculations using a different diffusivity. Cooling rates calculated in the Wadi Tayin section of the Oman ophiolite (this study) represent a range of two orders of magnitude. This range is in good agreement with the ranges presented by the numerical models of Cherkaoui et al. (2003) and Maclennan et al. (2004), as well as the range predicted by the geophysical model of Dunn et al. (2000). The cooling rates of Coogan et al. (2002) for the Wadi Abyad section of the Oman ophiolite, however, exhibit a much larger range (five orders of magnitude) and are inconsistent with predictions by numerical and geophysical models.

5.2.2. Geophysical models

Cooling rate data obtained by petrologic observation should be consistent not only with numerical simulations but also with geophysical observations. The Oman lower crust is thought to have formed at an intermediate-to fast-spreading ridge, and thus is compared to studies from the EPR (a fast spreading ridge). Using P-wave seismic tomography at the EPR, Dunn et al. (2000) inferred thermal anomalies and temperature gradients from the velocity structure to show that isotherms are nearly vertical and very closely spaced over a narrow region across the ridge axis (5–7 km). The inferred isotherms suggest that heat loss is very efficient throughout the lower crust at the EPR.

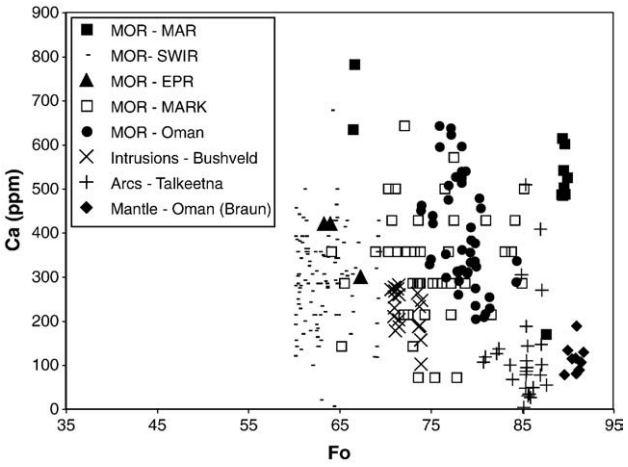

Fig. 8. Comparison of Ca contents of olivines from other spreading ridges. Oman=this study; MAR=Mid Atlantic Ridge (data from ODP Leg 209, unpublished data, P.B. Kelemen); MARK=Mid Atlantic Ridge at Kane Fracture Zone (Werner and Pilot, 1997); SWIR=Southwest Indian Ridge (Dick et al., 2002); EPR=East Pacific Rise (Natland and Dick, 1996); Bushveld layered mafic intrusion (unpublished data, J.A. VanTongeren); Talkeetna arc lower crust (unpublished data, K. Hanghøj). See text for discussion.

Author's personal copy

Cooling rates for the geophysical model of Dunn et al. (2000; Fig. 10 b) were calculated by digitizing the figure and measuring the distance from the 1200 °C isotherm to the 800 °C isotherm and multiplying by the 9'30N EPR half spreading rate (55 mm/year). The 800 °C isotherm was chosen in this case because the 700 °C isotherm does not extend to Moho depths. Cooling rate calculations based on Ca in olivine data from this study are systematically slightly faster than cooling rates based on thermal gradients reported by Dunn et al. (2000) for fast spreading ridges (Fig. 7). We are not aware of a comparable data set for intermediate-spreading ridges.

5.3. The role of hydrothermal circulation in the lower crust

As previously mentioned, hydrothermal circulation extending to the base of the crust is required to cool the lower crust at roughly the same rate at all depths. There have been many studies on the extent of hydrothermal circulation throughout the lower crust at the EPR and in the Oman ophiolite (see Section 2.3 for discussion). Data presented in this study (Fig. 4) require significant hydrothermal circulation to Moho depths at intermediate-fast spreading ridges, such as the Oman paleo-ridge. The sheeted sill model is therefore a thermally viable mechanism for crustal accretionary processes at mid ocean ridges. While the conclusions presented here do not rule out the possibility of accretion by gabbro glacier, they do contradict the initial tenet of the gabbro glacier model – convective heat loss by hydrothermal circulation *can* penetrate to Moho depths and crystallization is *not*, by necessity, constrained to the upper crust.

5.4. Comparison with present day ridges

The trend seen in cooling rates closely follows the trend exhibited by Ca in olivine analyses for this study (Fig. 4). It therefore may be possible to infer relative cooling rates from previously published data without detailed knowledge of grain sizes in order to compare cooling rates between fast and slow spreading ridges. Previously published olivine mineral analyses in lower gabbros at Hess Deep (EPR), the Southwest Indian Ridge (SWIR), and the Mid Atlantic Ridge (MAR and MARK, Kane fracture zone) are presented in Fig. 8. There does not appear to be any correlation between spreading rate and cooling rates of these gabbros as inferred from Ca in olivine. This could be a result of imprecise measurement by other studies relative to this one. Also, another potential complication associated with this comparison could arise from imprecise estimates of the igneous crystallization depth from dredged samples.

5.5. Comparison with other tectonic regimes

Following the same logic as in Section 5.4, application of the Ca-in-olivine geospeedometer to other tectonic regimes shows distinct differences between mid ocean ridges, arcs, and layered intrusions, as well as oceanic mantle (Fig. 8). As mentioned in Section 4, Calcium content in olivine in gabbros in this study is systematically higher than Ca in olivine in the underlying mantle section (Fig. 4). Gabbros from all mid- ocean ridges appear to cool more quickly than those from layered intrusions, such as the Bushveld Complex. In addition, arc lower crust records slower cooling than oceanic lower crust and layered intrusions, and has similar cooling rates to Oman ophiolite upper mantle.

6. Conclusions

Data presented here show no systematic variation of cooling rate with depth in the crustal section, and are thus inconsistent with conductive cooling models. Instead, the data indicate that hydrothermal cooling extended to the base of the crust within a few km of the ridge axis during formation of the Khafifah section in the Wadi Tayin massif of the Oman ophiolite.

Our results differ from a previous study of Ca in olivine in the lower crust in the Wadi Abyad section in the Nakhl massif of the Oman ophiolite by Coogan et al. (2002). Data of Coogan et al. (2002) extend to cooling rates slower than predicted in a purely conductive cooling model. The reason for this is unclear, however, it may be due to polygenetic magmatism and retrograde metamorphism of the base of the Wadi Abyad crustal section, or may arise from uncertainties in the characterization of D_o. Nonetheless, the range of values reported in this study for cooling rates in the lower crust is consistent with the range determined from both numerical and geophysical observations, whereas the range of values reported by Coogan et al. is more than two orders of magnitude larger. For this reason, we suggest more confidence be placed in the results presented in this study for cooling rates in the lower crust of the Oman paleo-ridge and, by proxy, all intermediate- to fast-spreading ridges.

The near-uniform cooling rates seen in our data suggest that hydrothermal circulation is an effective mechanism for heat loss during the formation of the entire lower oceanic crust. Most of the cooling rates for the lower crust measured in this study lie within the bounds of numerical calculations based on a combination of conductive and convective cooling. A number of our samples, however, record cooling rates faster than in models that include vigorous hydrothermal convection to the base of the crust. This may be due to emplacement of sills within previously cooled gabbroic rocks within a few km of the ridge axis. In this regard, our data are more consistent with the sheeted sill model for lower crust formation. Indeed, given the potential for igneous crystallization and solidification throughout a hydrothermally cooled lower crust, ductile flow of a magma mush, as required for the gabbro glacier model, seems comparatively unlikely.

Acknowledgments

The authors would like to thank C. MacLeod and J. Maclennan for their helpful and insightful reviews, as well as L.A. Coogan for providing inter-laboratory standards. J.V.T. thanks C. Mandeville for help with initial data collection, as well

Author's personal copy

as E.A. Mathez, and S. Goldstein for insightful discussions. Research was supported by NSF research grants OCE-0426160, OCE 0242233 and EAR-9910899. Lamont-Doherty Earth Observatory publication number 7110.

Appendix A. Supplementary data

Supplementary data associated with this article can be found, in the online version, at doi:10.1016/j.epsl.2007.11.034.

References

Alabaster, T., Pearce, J.A., Malpas, J., 1982. The volcanic stratigraphy and petrogenesis of the Oman ophiolite complex. Contrib. Mineral. Petrol. 81, 168–183.

Alt, J.C., Bach, W., 2006. Oxygen isotope composition of a section of lower oceanic crust, ODP Hole 735B. Geochem. Geophys. Geosys. 7.

Arai, S., Kadoshima, K., Morishita, T., 2006. Widespread arc-related melting in the mantle section of the northern Oman ophiolite as inferred from detrital chromian spinels. J. Geol. Soc. 163, 869–879.

Bosch, D., Jamais, M., Boudier, F., Nicolas, A., Dautria, J.-M., Agrinier, P., 2004. Deep and high-temperature hydrothermal circulation in the Oman ophiolite — petrological and isotopic evidence. J. Petrol. 45, 1181–1208.

Boudier, F., Coleman, R.G., 1981. Cross-section through the peridotite in the Samail Ophiolite, Southeastern Oman Mountains. J. Geophys. Res. 86, 2573–2592.

Boudier, F., Nicolas, A., Ildefonse, B., 1996. Magma chambers in the Oman ophiolite: fed from the top or the bottom? Earth Planet. Sci. Lett. 144, 239–250.

Braun, M.G., Petrologic and microstructural constraints on focused melt transport in dunites and the rheology of the shallow mantle, Ph.D., Joint Program in Oceanography/Applied Ocean Science and Engineering (Massachusetts Institute of Technology, Dept. of Earth, Atmospheric, and Planetary Sciences; and the Woods Hole Oceanographic Institution), 2004.

Buck, W.R., 2000. Can downward flow of dense cumulate slurry through mushy upper gabbros produce lower gabbros at a fast-spreading center? In: Dilek, Y., Moores, E.M., Elthon, D., Nicolas, A. (Eds.), Ophiolites and Oceanic Crust: New Insights from Field Studies and the Ocean Drilling Program, Geological Society of America Special Paper, vol. 349. Geological Society of America (GSA), Boulder, Colorado, pp. 121–127.

Cannat, M., 1996. How thick is the magmatic crust at slow spreading oceanic ridges? J. Geophys. Res. 101, 2847–2857.

Carbotte, S.M., Ryan, W.B.F., Jin, W., Cormier, M.H., Bergmanis, E., Sinton, J., White, S., 2003. Magmatic subsidence of the East Pacific Rise (EPR) at 18 degrees 14' S revealed through fault restoration of ridge crest bathymetry. Geochem. Geophys. Geosys. 4.

Chen, Y.J., 2001. Thermal effects of gabbro accretion from a deeper second melt lens at the fast spreading East Pacific Rise. J. Geophys. Res. 106, 8581–8588.

Cherkaoui, A.S.M., Wilcock, W.S.D., Dunn, R.A., Toomey, D.R., 2003. A numerical model of hydrothermal cooling and crustal accretion at a fast spreading mid-ocean ridge. Geochem. Geophys. Geosys. 4.

Collier, J.S., Singh, S.C., 1997. Detailed structure of the top of the melt body beneath the East Pacific Rise at 9 degrees 40'N from waveform inversion of seismic reflection data. J. Geophys. Res. 102, 20287–20304.

Coogan, L., Jenkin, G.R.T., Wilson, R.N., 2002. Constraining the cooling rate of the lower oceanic crust: a new approach applied to the Oman ophiolite. Earth Planet. Sci. Lett. 199, 127–146.

Coogan, L.A., Hain, A., Stahl, S., Chakraborty, S., 2005. Experimental determination of the diffusion coefficient for calcium in olivine between 900 degrees C and 1500 degrees C. Geochim. Cosmochim. Acta 69, 3683–3694.

Coogan, L.A., Howard, K.A., Gillis, K.M., Bickle, M.J., Chapman, H., Boyce, A.J., Jenkin, G.R.T., Wilson, R.N., 2006. Chemical and thermal constraints on focussed fluid flow in the lower oceanic crust. Amer. J. Sci. 306, 389–427.

Crawford, W.C., Webb, S.C., 2002. Variations in the distribution of magma in the lower crust and at the Moho beneath the East Pacific Rise at 9 degrees–10 degrees N. Earth Planet. Sci. Lett. 203, 117–130.

Crawford, W.C., Webb, S.C., Hildebrand, J.A., 1999. Constraints on melt in the lower crust and Moho at the East Pacific Rise, 9 degrees 48' N, using seafloor compliance measurements. J. Geophys. Res. 104, 2923–2939.

Dalton, J.A., Lane, S.J., 1996. Electron microprobe analysis of Ca in olivine close to grain boundaries: the problem of secondary X-ray fluorescence. Am. Mineral. 81, 194–201.

Detrick, R.S., Buhl, P., Vera, E., Mutter, J., Orcutt, J., Madsen, J., Brocher, T., 1987. Multi-channel seismic imaging of a crustal magma chamber along the East Pacific Rise. Nature 326, 35–41.

Dick, H.J.B., Ozawa, K., Meyer, P.S., Niu, Y., Robinson, P.T., Constantin, M., Hebert, R., Maeda, J., Natland, J.H., Hirth, J.G., Mackie, S.M., 2002. Primary silicate mineral chemistry of a 1.5-km section of very slow spreading lower ocean crust: ODP Hole 735B, Southwest Indian Ridge. In: Natland, J.H., Dick, H.J.B., Miller, D.J., Von Herzen, R.P. (Eds.), Proc. ODP, Sci. Results, vol. 176. College Station, TX (Ocean Drilling Program), pp. 1–60.

Dodson, M.H., 1973. Closure temperature in cooling geochronological and petrological systems. Contrib. Mineral. Petrol. 40, 259–274.

Dunn, R.A., Toomey, D.R., Solomon, S.C., 2000. Three-dimensional seismic structure and physical properties of the crust and shallow mantle beneath the East Pacific Rise at 9 degrees 30'N. J. Geophys. Res. 105, 23537–23555.

Ehlers, K., Powell, R., Stuwe, K., 1994. Cooling rate histories from garnet+ biotite equilibrium. Am. Mineral. 79, 737–744.

Fisher, A.T., 1998. Permeability within basaltic oceanic crust. Rev. Geophys. 36, 143–182.

Garrido, C.J., Kelemen, P.B., Hirth, G., 2001. Variation of cooling rate with depth in lower crust formed at an oceanic spreading ridge: plagioclase crystal size distributions in gabbros from the Oman ophiolite. Geochem. Geophys. Geosys. 2.

Gregory, R.T., Taylor, H.P., 1981. An oxygen isotope profile in a section of Cretaceous oceanic crust, Samail Ophiolite, Oman: evidence of del18O buffering of the oceans by deep (>5 km) seawater-hydrothermal circulation at mid-ocean ridges. J. Geophys. Res. 86, 2737–2755.

Hanghoj, K., Kelemen, P.B., Hassler, D., Rudnick, R., Godard, M., Walker, R., in preparation. Composition and genesis of depleted mantle peridotites from the wadi tayin massif, Oman ophiolite. Major and trace element geochemistry, and Os isotope and PGE systematics.

Harding, A.J., Orcutt, J., Kappus, M., Vera, E., Mutter, J., Buhl, P., Detrick, R., Brocher, T., 1989. The structure of young oceanic crust at 13N on the East Pacific Rise from expanding spread profiles. J. Geophys. Res. 94, 12163–12196.

Henstock, T.J., Woods, A.W., White, R.S., 1993. The accretion of oceanic-crust by Episodic Sill intrusion. J. Geophys. Res. 98, 4143–4161.

Hooft, E.E.E., Detrick, R.S., Kent, G.M., 1997. Seismic structure and indicators of magma budge along the southern East Pacific Rise. J. Geophys. Res. 102, 27319–27340.

Hussenoeder, S.A., Collins, J.A., Kent, G.M., Detrick, R.S., Harding, A.J., Orcutt, J.A., Mutter, J.C., Buhl, P., 1996. Seismic analysis of the axial magma chamber reflector along the southern East Pacific Rise from conventional reflection profiling. J. Geophys. Res. 101, 22087–22105.

Jurewicz, A.J.G., Watson, E.B., 1988. Cations in olivine, Part 2: diffusion in olivine xenocrysts, with applications to petrology and mineral physics. Contrib. Mineral. Petrol. 99, 186–201.

Juteau, T., Ernewein, M., Reuber, I., Whitechurch, H., Dahl, R., 1988a. Duality of magmatism in the plutonic sequence of the Sumail nappe, Oman. Tectonophysics 151, 107–135.

Juteau, T., Beurrier, M., Dahl, R., Nehlig, P., 1988b. Segmentation at a fossil spreading axis: the plutonic sequence of the Wadi Haymiliyah area (haylayn block, Sumail Nappe, Oman). Tectonophysics 51, 167–197.

Kawahata, H., Nohara, M., Ishizuka, H., Hasebe, S., Chiba, H., 2001. Sr isotope geochemistry and hydrothermal alteration of the Oman ophiolite. J. Geophys. Res. 106, 11083–11099.

Kelemen, P.B., Aharonov, E., 1998. Periodic formation of magma fractures and generation of layered gabbros in the lower crust beneath oceanic spreading ridges. Geophys. Monograph. AGU 106, 267–289.

Author's personal copy

Kelemen, P.B., Koga, K., Shimizu, N., 1997. Geochemistry of gabbro sills in the crust/mantle transition zone of the Oman ophiolite: Implications for the origin of the oceanic lower crust. Earth Planet. Sci. Lett. 146, 475–488.

Kohler, T.P., Brey, G.P., 1990. Calcium exhange between olivine and clinopyroxene calibrated as a geothermometer for natural peridotites from 2 to 60 kb with applications. Geochim. Cosmochim. Acta 54, 2375–2388.

Korenaga, J., Kelemen, P.B., 1998. Melt migration through the oceanic lower crust: a constraint from melt percolation modeling with finite solid diffusion. Earth Planet. Sci. Lett. 156, 1–11.

Korenaga, J., Kelemen, P.B., 1997. The origin of gabbro sills in the Moho transition zone of the Oman ophiolite: Implications for magma transport in the oceanic lower crust. J. Geophys. Res. 102, 27,729–727,749.

Lachize, M., Lorand, J.P., Juteau, T., 1996. Calc-alkaline differentiation trend in the plutonic sequence of the Wadi Haymiliyah section, Haylayn massif, Semail ophiolite, Oman. Lithos 38, 207–232.

Lanphere, M.A., Coleman, R.G., Hopson, C.A., 1981. Sr Isotopic Tracer Study of the Samail Ophiolite, Oman. J. Geophys. Res. 86, 2709–2720.

Lecuyer, C., Reynard, B., 1996. High temperature alteration of oceanic gabbros by seawater (Hess Deep, Ocean Drilling Program Leg 147): evidence from oxygen isotopes and elemental fluxes. J. Geophys. Res. 101, 15883–15897.

Lewis, B.T.R., Garmany, J.D., 1982. Constraints on the structure of the East Pacific Rise from Seismic refraction data. J. Geophys. Res. 87, 8417–8425.

Libourel, G., 1999. Systematics of calcium partioning between olivine and silicate melt: Implications for melt structure and calcium content of magmatic olivines. Contrib. Mineral. Petrol. 136, 63–80.

Longhi, J., Walker, D., Hays, J.F., 1978. The distribution of Fe and Mg between olivine and lunar basaltic liquids. Geochim. Cosmochim. Acta 42, 1545–1558.

Maclennan, J., Hulme, T., Singh, S.C., 2004. Thermal models of oceanic crustal accretion: Linking geophysical, geological and petrological observations. Geochem. Geophys. Geosys. 5.

Maclennan, J., Hulme, T., Singh, S.C., 2005. Cooling of the lower oceanic crust. Geology 33, 357–360.

MacLeod, C.J., Yaouancq, G., 2000. A fossil melt lens in the Oman ophiolite: implications for magma chamber processes at fast spreading ridges. Earth Planet. Sci. Lett. 176, 357–373.

McCulloch, M.T., Gregory, R.T., Wasserburg, G.J., Taylor, H.P., 1981. Sm–Nd, Rb–Sr, and O–18–O–16 isotopic systematics in an oceanic crustal section — evidence from the Samail Ophiolite. J. Geophys. Res. 86, 2721–2735.

Mevel, G., Faidy, C., Prieur, D., 1996. Distribution, activity, and diversity of heterotrophic nitrifiers originating from East Pacific deep-sea hydrothermal vents. Can. J. Microbiol. 42, 162–171.

Morioka, M., 1981. Cation diffusion in olivine-II. Ni–Mg, Mn–Mg, Mg and Ca. Geochim. Cosmochim. Acta 45, 1573–1580.

Morton, J.L., Sleep, N.H., 1985. A mid-ocean ridge thermal-model-constraints on the volume of axial hydrothermal heat-flux. J. Geophys. Res.-Solid Earth Planets 90, 1345–1353.

Natland, J.H., Dick, H.J.B., 1996. Melt migration through high-level gabbroic cumulates of the East Pacific Rise at Hess Deep: the origin of magma lenses and the deep crustal structure of fast-spreading ridges. In: Mével, C., Gillis, K.M., Allan, J.F., Meyer, P.S. (Eds.), Proc. ODP, Sci. Results, vol. 147. College Station, TX (Ocean Drilling Program), pp. 21–58.

Nedimovic, M.R., Carbotte, S.M., Harding, A.J., Detrick, R.S., Canales, J.P., Diebold, J.B., Kent, G.M., Tischer, M., Babcock, J.M., 2005. Frozen magma lenses below the oceanic crust. Nature 436, 1149–1152.

Nehlig, P., 1994. Fracture and permeability analysis in magma–hydrothermal transition zones in the Samail Ophiolite (Oman). J. Geophys. Res. 99, 589–601.

Nicolas, A., 1992. Kinematics in magmatic rocks with special reference to gabbros. J. Petrol. 33, 891–915.

Nicolas, A., Reuber, I., Benn, K., 1988. A new magma chamber model based on structural studies in the Oman ophiolite. Tectonophysics 151, 87–105.

Nicolas, A., Freydier, C., Godard, M., Vauchez, A., 1993. Magma chambers at oceanic ridges: How large? Geology 21, 53–56.

Nicolas, A., Boudier, E., Ildefonse, B., Ball, E., 2000. Accretion of Oman and United Arab Emirates ophiolite- Discussion of a new structural map Marine. Geophys. Res. 21, 147–179.

Nicolas, A., Mainprice, D., Boudier, F., 2003. High-temperature seawater circulation throughout crust of oceanic ridges: A model derived from the Oman ophiolites. J. Geophys. Res. 108.

Ozawa, K., 1984. Olivine-Spinel Geospeedometry — analysis of diffusion-controlled Mg–Fe-2+exchange. Geochim. Cosmochim. Acta 48, 2597–2611.

Pallister, J.S., Hopson, C.J., 1981. Samail ophiolite plutonic suite: field relations, phase variation, cryptic variation and layering, and a model of a spreading ridge magma chamber. J. Geophys. Res. 86, 2593–2644.

Pallister, J.S., Knight, R.J., 1981. Rare-earth element geochemistry of the Samail ophiolite near Ibra, Oman. J. Geophys. Res. 86, 2673–2697.

Pearce, J.A., Alabaster, T., Shelton, A.W., Searle, M.P., 1981. The Oman ophiolite as a cretaceous arc-basin complex: evidence and implications. Philos. Trans. R. Soc. Lond. A 300, 299–317.

Phipps Morgan, J., Chen, Y.J., 1993. The genesis of oceanic crust-magma injection, hydrothermal cooling, and crustal flow. J. Geophys. Res. 98, 6283–6297.

Quick, J.E., Denlinger, R.P., 1993. Ductile deformation and the origin of layered gabbro in ophiolites. J. Geophys. Res. 98, 14015–14027.

Roeder, P., 1974. Activity of iron and olivine solubility in basaltic liquids. Earth Planet. Sci. Lett. 23, 397–410.

Schouten, H., Denham, C., 1995. Virtual ocean crust. EOS Trans. AGU 76, S48.

Singh, S., Kent, G.M., Collier, J.S., Harding, A.J., Orcutt, J.A., 1998. Melt to mush variations in crustal magma properties along the ridge crest at the southern East Pacific Rise. Nature 394, 874–878.

Singh, S., Collier, J.S., Harding, A.J., Kent, G.M., Orcutt, J.A., 1999. Seismic evidence for a hydrothermal layer above the solid roof of the axial magma chamber at the southern East Pacific Rise. Geology 27, 219–222.

Singh, S.C., Harding, A.J., Kent, G.M., Sinha, M.C., Combier, V., Bazin, S., Tong, C.H., Pye, J.W., Barton, P.J., Hobbs, R.W., White, R.S., Orcutt, J.A., 2006. Seismic reflection images of the Moho underlying melt sills at the East Pacific Rise. Nature 442, 287–290.

Smewing, J.D., 1981. Mixing characteristics and compositional differences in mantle-derived melts beneath spreading axes: evidence from cyclically layered rocks in the ophiolite of North Oman. J. Geophys. Res. 86, 2645–2660.

Stahl, S., Hain, A., Chakraborty, S., Laqua, W., Palme, H., 1998. Tracer diffusion of 42Ca in olivine as a function of composition and pO_2 between 800 and 1500 degrees C. EOS Trans. AGU 79, 5370.

Stakes, D., Vanko, D.A., 1986. Multistage hydrothermal alteration of gabbroic rocks from the failed mathematician ridge. Earth Planet. Sci. Lett. 79, 75–92.

Tamura, A., Arai, S., 2006. Harzburgite-dunite-orthopyroxenite suite as a record of supra-subduction zone setting for the Oman ophiolite mantle. Lithos 90, 43–56.

Tilton, G.R., Hopson, C.A., Wright, J.E., 1981. Uranium-lead isotopic ages of the Samail Ophiolite, Oman, with applications to Tethyan ocean ridge tectonics. J. Geophys. Res. 86, 2763–2775.

Toomey, D.R., Purdy, G.M., Solomon, S., Wilcock, W., 1990. The three dimensional seismic velocity structure of the East Pacific Rise near latitude 9 30N. Nature 347, 639–644.

Vera, E.E., Mutter, J.C., Buhl, P., Orcutt, J.A., Harding, A.J., Kappus, M.E., Detrick, R.S., Brocher, T.M., 1990. The Structure of 0-My to 0.2-My Old Oceanic–Crust at 9-Degrees-N on the East Pacific Rise from expanded spread profiles. J. Geophys. Res.-Solid Earth Planets 95, 15529–15556.

Werner, C.-D., Pilot, J., 1997. Data report: geochemistry and mineral chemistry of ultramafic rocks from the Kane area (MARK). In: Karson, J.A., Cannat, M., Miller, D.J., Elthon, D. (Eds.), Proc. ODP, Sci. Results, vol. 153. College Station, TX (Ocean Drilling Program), pp. 457–470.